

Ag^I/V^V Heterobimetallic Frameworks Generated from Novel-Type {Ag₂(VO₂F₂)₂(triazole)₄} Secondary Building Blocks: A New Aspect in the Design of SVOF Hybrids

Ganna A. Senchyk,[†] Valeriy O. Bukhan'ko,[†] Andrey B. Lysenko,^{*,†} Harald Krautscheid,[‡] Eduard B. Rusanov,[§] Alexandr N. Chernega,[§] Mirosław Karbowski,^{||} and Konstantin V. Domasevitch[†]

[†]Inorganic Chemistry Department, National Taras Shevchenko University of Kyiv, Volodimirska Street 64, Kyiv 01033, Ukraine

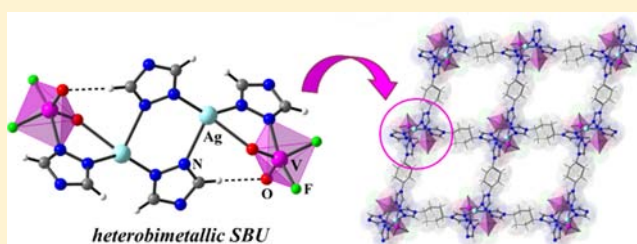
[‡]Institut für Anorganische Chemie, Universität Leipzig, Johannisallee 29, D-04103 Leipzig, Germany

[§]Institute of Organic Chemistry, Murmanska Street 5, Kyiv, 02660, Ukraine

^{||}Faculty of Chemistry, University of Wrocław, 14 Joliot-Curie Street, 50-383 Wrocław, Poland

S Supporting Information

ABSTRACT: A series of new silver(I)-containing MOFs [Ag₂(tr₂ad)₂](ClO₄)₂ (1), [Ag₂(VO₂F₂)₂(tr₂ad)₂] \cdot H₂O (2), [Ag₂(VO₂F₂)₂(tr₂eth)₂](H₂O)₂ (3), and [Ag₂(VO₂F₂)₂(tr₂cy)₂] \cdot 4H₂O (4) supported by 4-substituted bifunctional 1,2,4-triazole ligands (tr₂ad = 1,3-bis(1,2,4-triazol-4-yl)adamantane, tr₂eth = 1,2-bis(1,2,4-triazol-4-yl)ethane, tr₂cy = *trans*-1,4-bis(1,2,4-triazol-4-yl)cyclohexane) were hydrothermally synthesized and structurally characterized. In these complexes, the triazole heterocycle as an N¹,N²-bridge links either two adjacent Ag–Ag or Ag–V centers at short distances forming polynuclear clusters. The crystal structure of compound 1 is based on cationic {Ag₂(tr)₄}²⁺ fragments connected in a 2D rhombohedral grid network with (4,4) topology. The neighboring layers are tightly packed into a 3D array by means of argentophilic interactions (Ag \cdots Ag 3.28 Å). Bridging between different metal atoms through the triazole groups assists formation of heterobimetallic Ag^I/V^V secondary building blocks in a linear V–Ag–Ag–V sequence that is observed in complexes 2–4. These unprecedented tetranuclear {Ag₂(VO₂F₂)₂(tr)₄} units (the intermetal Ag–Ag and Ag–V distances are 4.24–4.36 and 3.74–3.81 Å, respectively), in which vanadium(V) oxofluoride units possess distorted trigonal bipyramidal environment {VO₂F₂N}⁺, are incorporated into 1D ribbon (2) or 2D square nets (3, 4) using bitopic μ_4 -triazole ligands. The valence bond calculation for vanadium atoms shows +V oxidation state in the corresponding compounds. Thermal stability and photoluminescence properties were studied for all reported coordination polymers.



INTRODUCTION

Heterobimetallic secondary building units (SBUs), where two different metal centers are connected through a short bridge, have great potential for construction of metal–organic polymers¹ with nontrivial magnetic, optical, luminescent, and catalytic behavior.² In this context, simultaneous incorporation of early and late transition metal ions into the framework develops a highly fascinating trend toward solid materials. Among them, organic–inorganic hybrid solids containing a vanadium oxofluoride (VOF) matrix are of particular interest presenting an enormous diversity of types and structural motifs.^{3–25} In spite of considerable efforts made in this field the main success was achieved in synthesis of simple VOF salts with organic charge-compensating cations^{4–18,20,21} (Table 1). Integration of VOF anions into coordination polymers, where they play a bridging role or are a structurally important part of the framework, represents an impressive advantage. For instance, silver(I)-containing VOFs (SVOFs, Ag₄V₂O₆F₂²⁶ and Ag₃VO₂F₄²⁷) received much attention as electrochemically

active phases for solid-state battery applications. At the same time, mixed-metal Ag^I/V^V hybrids show photocatalytic activity in the light-driven production of H₂ and/or O₂ in aqueous solutions arising from a metal-to-metal charge transfer (MMCT) between the d¹⁰ and the d⁰ electron configurations.²⁸ However, only a few VOF examples with direct ligation of organic N-donor chelates have been reported so far^{22–25} (see Table 1).

Azole heterocycles with two neighboring N-donor atoms (pyrazole, triazole, tetrazole) offer many attractive opportunities in bridging of metal centers into polynuclear fragments. Such functional groups show high affinity not only toward late transition metals (Cu, Ag, etc.) but also to early transition metal oxide/oxofluoride species (MoO₃, etc.). It suggests the possibility to form heterometallic compounds by means of N,N-bridging. However, this idea is confirmed only by several

Received: January 13, 2012

Published: July 25, 2012

Table 1. Vanadium Oxo–Fluoride (VOF) Compounds Previously Reported and Structurally Characterized

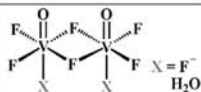
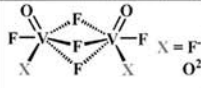
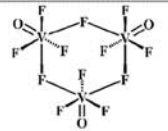
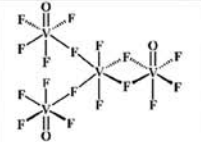
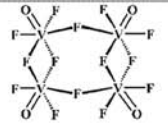
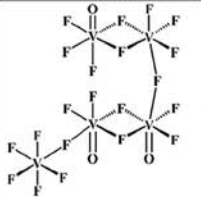
Compound	Anionic polyhedra	Oxid. state	Structural features	Ref.
VOF salts with organic cations				
[enH ₂][VOF ₅] [*]	VOF ₅	+ 5	Inorganic anion, octahedra	4
[detaH ₃][VOF ₅] [*]		+ 4		5
[tetaH ₄][VF ₅ (H ₂ O)] [*]		+ 3		5
[enH ₂][VOF ₄ (H ₂ O)] [*]	VO ₂ F ₄	+ 4	Inorganic anion, octahedra	6
[pipH ₂][VOF ₄ (H ₂ O)] [*]				7
[tetaH ₄][VOF ₄ (H ₂ O)] ₂ ·H ₂ O [*]				5
[NMe ₄] ₂ [V ₂ O ₂ F ₆ (H ₂ O) ₂]		+ 4	Inorganic anion, edge-shared octahedra	8
[NEt ₄] ₂ [V ₂ O ₂ F ₆ (H ₂ O) ₂]		+ 4		9
[4,4'-bipyH ₂][V ₂ O ₂ F ₆ (H ₂ O) ₂] [*]		+ 4		5
[dabcoH ₂][V ₂ O ₂ F ₆ (H ₂ O) ₂] [*]		+ 4		5
[tetaH ₄][V ₂ O ₂ F ₈] [*]		+ 4		5
[pipH ₂] ₃ [V ₂ O ₂ F ₈][VOF ₄ (H ₂ O)] ₂ [*]		+ 4, + 5		7
[NMe ₄] ₃ [V ₂ O ₄ F ₅]		+ 5	Inorganic anion, face-shared octahedra	10
[NMe ₄] ₃ [V ₂ O ₂ F ₇]		+ 4		11
K[NMe ₄] ₂ [V ₃ O ₃ F ₁₂]		+ 5	Inorganic anion, corner-shared octahedra	12
[pipH ₂] ₄ [V ₄ O ₃ F ₁₇] ₂ ·4H ₂ O [*]		+ 3, + 4	Inorganic anion, corner- and edge-shared octahedra	7
[trenH ₃] ₂ [V ₄ O ₄ F ₁₄] ₂ ·3H ₂ O [*]		+ 4	Inorganic anion, corner- and edge-shared octahedra	5
[adapH ₃] ₂ [V ₄ O ₄ F ₁₄] ₂ ·2H ₂ O [*] (isomeric form)				5
[pipH ₂] ₄ [V ₅ O ₃ F ₂₀] ₂ ·2H ₂ O [*]		+ 3, + 4	Inorganic anion, corner- and edge-shared octahedra	7
[1,5-dapH ₂] ₄ [V ₁₄ O ₃₆ F ₄] ₂ ·8H ₂ O [*]	VO ₆ , VO ₅ F	+ 4, + 5	Polyoxofluorovanadate anion	13
[1,6-dahH ₂] ₄ [V ₁₄ O ₃₆ F ₄] ₂ ·4H ₂ O [*]				
[VF ₃ (H ₂ O) ₂]	VO ₂ F ₄	+ 3	Chain, corner-shared octahedra	14
[enH ₂][VOF ₄] [*]	VOF ₅	+ 4	Chain, corner-shared octahedra	14

Table 1. continued

Compound	Anionic polyhedra	Oxid. state	Structural features	Ref.
VOF salts with organic cations				
[bpeH ₂] _{0.5} [VOF ₃ (H ₂ O)] [*]	VO ₂ F ₄	+ 4	Chain, corner-shared octahedra	15
[pyH][V ₂ O ₂ F ₅] [*]	VOF ₅	+ 4	Double chain, corner- and edge-shared octahedra	16
[bpeH ₂] _{0.5} [VOF ₃] [*]		+ 4		17
VOF coordination compounds				
[pyH] ₂ [Cu(py) ₄ (VOF ₅) ₂] [*]	VOF ₅	+ 5	Molecular complex	18
[Cu(py) ₄ (VOF ₄)] ₂ [Cu(py) ₄ (H ₂ O)(VOF ₄)]·H ₂ O	VOF ₄	+ 4	1D chain and molecular fragment	19
[Cu(py) ₄ (VOF ₄)] [*]	VOF ₄	+ 4	1D chain	19
[CH ₃ NH ₃] ₈ [Cu(py) ₄] ₃ [V ₇ O ₆ F ₃₀] [*]	VF ₆ , VOF ₅	+ 4	3D coordination polymer	20
[Me ₂ NH ₂][Cu(py) ₄ (V ₂ O ₂ F ₇)] [*]	VOF ₅ (face-shared dimer)	+ 4	1D chain	21
[Cu(im) ₄ (V ₂ O ₂ F ₈)]·2im [*]	VOF ₅ (edge-shared dimer)	+ 4	1D chain	21
Neutral VOFs with N-donor ligands				
[VO ₂ F(py) ₂] [*]	VO ₂ FN ₂	+ 5	Molecular topology	22
[VOF ₂ (1,10-phen)(H ₂ O)] [*]	VO ₂ F ₂ N ₂	+ 5	Molecular topology	22, 23
[V ₂ O ₄ F ₂ (2,2'-bipy) ₂] [*]	VO ₃ FN ₂	+ 5	Molecular topology	22, 24
[V ₂ O ₄ F ₂ (1,10-phen) ₂] [*]	VO ₃ FN ₂	+ 5	Molecular topology	25

* Abbreviations: mono (py = pyridine), di (en = ethylenediamine; 4,4'-bipy = 4,4'-bipyridine; dabco = 1,4-diazabicyclo[2.2.2]octane; pip = piperazine; bpe = *trans*-1,2-bis(4-pyridyl)ethylene; 1,5-dap = 1,5-diaminopentane; 1,6-dah = 1,6-diaminohexane), tri (deta = diethylenetriamine; tren = tris(2-aminoethyl)amine; adap = *N*-(3-aminopropyl)-1,3-diaminopropane); tetraprotonated species (teta = triethylenetetramine or 1,4,7,10-tetraazadecane); im = imidazole; 1,10-phen = 1,10-phenanthroline; 2,2'-bipy = 2,2'-bipyridine.

metal–organic hybrids where acido–tetrazolate derivatives connect d-element atoms with the molybdenum–oxide matrix.²⁹ In the case of neutral 1,2,4-triazole ligands, the assembly of metal oxide– or oxo–fluoride–organic frameworks (MOOFs) is the result of strong cooperation between *N,N*-azole and short covalent oxo bridges.³⁰

At first glance, it is surprising that a symmetrical triazole ring, having two equivalent donor sites (N1 and N2), can simultaneously and selectively interact with different metal types. The situation essentially changes in metal clusters with free donor centers, that is often observed in silver–triazole systems. From Scheme 1 it becomes evident that the simplest {Ag₂(η²-tr)₂(tr)₂}²⁺ binuclear cationic fragment is unsaturated (two N atoms remain noncoordinating) and has a potential for further interactions as a Lewis base. On the other hand, a big variety of vanadium oxo–fluoride anions (mononuclear {VOF₄(H₂O)}₁,^{5–7} binuclear {V₂O₂F₆(H₂O)₂}^{8,9} and {V₂O₂F₈(H₂O)}₁₂ or polymeric^{14,15}) contain a weakly coordinated water molecule, very labile toward N-donor ligand substitution, and can behave as Lewis acids. Thus, the rational combination between the dicationic {Ag₂(η²-tr)₂(tr)₂}²⁺ donor

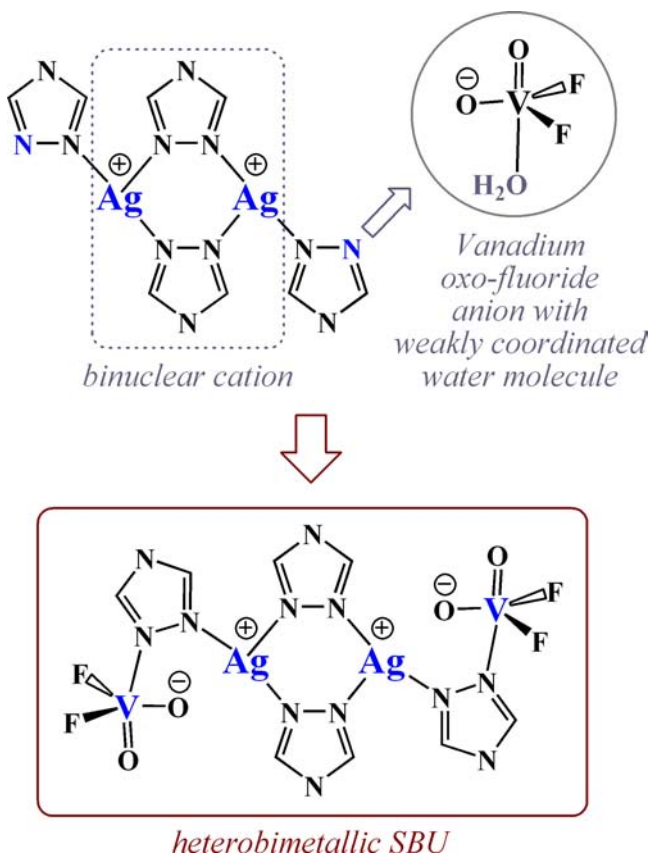
and two charge-compensating VO₂F₂(H₂O)[−] acceptors affords the tetranuclear unit {Ag₂(VO₂F₂)₂} supported by four triazole bridges.

In the present article we introduce the design principles toward novel Ag^I/VOF heterobimetallic complexes based on the {Ag₂(VO₂F₂)₂(tr)₄} SBUs, which are integrated into MOFs employing bitopic 1,2,4-triazole ligands with aliphatic linkers: flexible 1,2-ethanediyl, semirigid linear *trans*-1,4-cyclohexanediyl, and rigid angular 1,3-adamantanediyl (Scheme 2). Following this strategy, the compounds were successfully prepared in high yields by a simple ‘one-pot’ hydrothermal methodology.

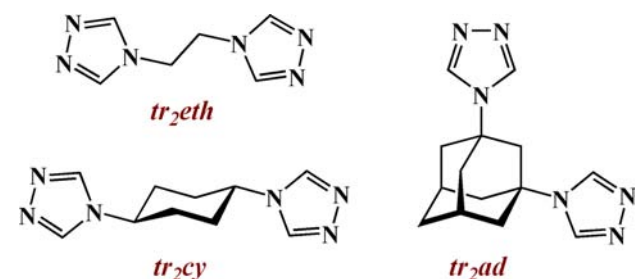
EXPERIMENTAL SECTION

Synthesis of Organic Ligands. All chemicals were of reagent grade and used as received without further purification. 1,2,4-Triazole ligands were prepared in yields up to 60% by the general synthetic procedure: refluxing of the corresponding diamines (ethane-1,2-diamine, *trans*-cyclohexane-1,4-diamine, adamantane-1,3-diamine) with *N,N*-dimethylformamide azine in xylene/toluene in the presence of *p*-toluenesulfonic acid monohydrate as the catalyst.^{30,31}

Scheme 1. New Approach to ‘One-Pot’ Synthesis of Heterometallic Ag/VOF Coordination Polymers That Promotes Formation of Novel Tetranuclear SBUs Supported by 1,2,4-Triazole Bridges



Scheme 2. Bitopic 1,2,4-Triazole Ligands with Aliphatic Spacers, Flexible Linear (*tr₂eth*), Semi-Rigid Linear (*tr₂cy*), and Rigid Angular (*tr₂ad*) Platform, Utilized in the Presented Study



Synthesis of Coordination Compounds. *Caution:* HF (50%) is toxic and corrosive and must be handled in a well-ventilated fume hood with extreme caution using appropriate protective gear!

All complexes were prepared under hydrothermal conditions as follows. A mixture of the components and distilled water was placed into a 20 mL Teflon-lined steel autoclave, stirred for 30 min, and heated in an oven at the temperature range of 150–180 °C for 24–40 h, with further cooling to room temperature (cooling rate 2–2.5 °C/h). Crystalline products were collected, washed with water and methanol, and dried in air.

$[Ag_2(tr_2ad)_2](ClO_4)_2$ (**1**). A mixture of $AgClO_4$ (15.4 mg, 0.074 mmol), *tr₂ad* (10.0 mg, 0.037 mmol), and 5 mL of water was placed in a Teflon reactor and heated at 180 °C for 40 h. Cooling to room temperature during the next 60 h led to colorless prisms of the product in 24.7 mg yield (70%). Anal. Calcd for $C_{28}H_{36}Ag_2Cl_2N_{12}O_8$: C, 35.20;

H, 3.80; N, 17.59. Found: C, 35.25; H, 3.68; N, 17.47. IR (KBr discs, selected bands, cm^{-1}): 624s, 640s, 666m, 728m, 850m, 884m, 986s, 1094s, 1196s, 1238m, 1290m, 1326s, 1340m, 1370m, 1456m, 1520s, 2868m, 2916m, 2948m, 3128s.

$[Ag_2(VO_2F_2)_2(tr_2ad)_2] \cdot H_2O$ (**2**). A mixture of $AgOAc$ (13.6 mg, 0.074 mmol), *tr₂ad* (10.0 mg, 0.037 mmol), and V_2O_5 (6.7 mg, 0.037 mmol) was added to 5 mL of water with aqueous HF (50%, 100 μ L, 2.89 mmol) in a Teflon vessel. The sealed reactor was kept at 165 °C for 24 h and then slowly cooled to room temperature during 50 h, yielding 16.2 mg (87%) of big light-yellow prismatic crystals. Anal. Calcd for $C_{28}H_{38}Ag_2F_4N_{12}O_5V_2$: C, 33.09; H, 3.77; N, 16.54. Found: C, 32.98; H, 3.80; N, 16.51. IR (KBr discs, selected bands, cm^{-1}): 532s, 536m, 658s, 734m, 854m, 918s, 1030m, 1072s, 1200s, 1324m, 1366m, 1464m, 1526s, 2858m, 2924s, 2986m, 3028m, 3080s, 3116m, 3434m.

$[Ag_2(VO_2F_2)_2(tr_2eth)_2(H_2O)_2]$ (**3**). A mixture of $AgOAc$ (16.7 mg, 0.100 mmol), *tr₂eth* (16.4 mg, 0.100 mmol), V_2O_5 (9.1 mg, 0.050 mmol), and 5 mL of water with aqueous HF (50%, 150 μ L, 4.33 mmol) was placed in a Teflon vessel. The reactor was heated at 150 °C for 24 h and cooled to room temperature during 50 h, leading to yellowish crystalline product in 27.2 mg yield (73%). Anal. Calcd for $C_{12}H_{20}Ag_2F_4N_{12}O_6V_2$: C, 17.53; H, 2.45; N, 20.45. Found: C, 17.61; H, 2.42; N, 20.37. IR (Nujol, selected bands, cm^{-1}): 570w, 640s, 684m, 722m, 878s, 910s, 964s, 998m, 1036m, 1082s, 1172s, 1200s, 1332m, 1378s, 1462s, 1540s, 1668m, 2674m, 2724m, 3112m, 3154m, 3228m.

$[Ag_2(VO_2F_2)_2(tr_2cy)_2] \cdot 4H_2O$ (**4**). A mixture of $AgOAc$ (16.7 mg, 0.100 mmol), *tr₂cy* (10.9 mg, 0.050 mmol), V_2O_5 (9.1 mg, 0.050 mmol), and 5 mL of water with aqueous HF (50%, 150 μ L, 4.33 mmol) was added into a Teflon vessel. Then the components were heated at 150 °C for 24 h and slowly cooled to room temperature during 50 h, yielding 20.3 mg (84%) of light-yellow prismatic crystals. Anal. Calcd for $C_{20}H_{36}Ag_2F_4N_{12}O_8V_2$: C, 24.86; H, 3.76; N, 17.40. Found: C, 24.79; H, 3.85; N, 17.25. IR (Nujol, selected bands, cm^{-1}): 576m, 652s, 722m, 802m, 916s, 950s, 978m, 992m, 1014m, 1028m, 1046s, 1088s, 1190s, 1216s, 1238m, 1306m, 1352s, 1376s, 1406m, 1444s, 1470s, 1540s, 1634m, 2672m, 2724m, 2832s, 2988s, 3094s, 3180m, 3444m.

Measurements. Elemental analysis was carried out with a Vario EL-Heraeus microanalyzer.

IR spectra (400–4000 cm^{-1}) were collected using a Perkin-Elmer FTIR spectrometer on KBr discs and Nujol for all compounds. IR spectra recorded as Nujol mulls were identical to those recorded in KBr, except for the Nujol absorptions.

X-ray powder diffraction was carried out on a Shimadzu XRD-6000 (Cu $K\alpha$ radiation) and Stoe STADIP (Cu $K\alpha_1$) using a linear PSD detector. Temperature-dependent X-ray measurements were carried out on a Stoe STADIP with a high-temperature attachment and image plate detector system.

Diffuse reflectance spectra were recorded in the 800–200 nm range at 298 K on a Cary-500 UV–vis–NIR spectrophotometer. Corrected emission and excitation spectra were recorded at 298 and 77 K on an Edinburgh Instruments FLSP 920 spectrofluorometer using the Optistat DN liquid nitrogen cryostat (Oxford Instrument).

X-ray Crystallography. Diffraction data were collected at 213 K using a Stoe Imaging Plate Diffraction System for **2** (numerical absorption correction) and at 100 K on a Bruker APEXII CCD area-detector diffractometer (φ scans) for **1**, **3**, and **4** (graphite-monochromated Mo $K\alpha$ radiation, $\lambda = 0.71073$ Å). Data were corrected for Lorentz-polarization effects and the effects of absorption (multiscans method). Structures were determined by direct methods and refined by full-matrix least-squares on F^2 using the SHELX-97 package.³² CH hydrogen atoms were placed in calculated positions and refined as fixed contributions with $U_{iso} = 1.2U_{eq}(C)$, while OH hydrogen atoms were located and then fixed at $O-H = 0.85$ Å and with $U_{iso} = 1.5U_{eq}(O)$. In **1**, the oxygen atoms of ClO_4^- are unequally disordered with partial occupancy factors 0.7 and 0.3. Disorder was resolved with restrained geometry for both contributions, while atoms of the minor component were left isotropic and refined with equal atomic displacement parameters. In **3**, the organic ligands adopt two closely separated orientations and are equally disordered. The

disordered portion was refined anisotropically without restraints in geometry, and hydrogen atoms were added with partial occupancies of 0.5. Crystallographic data and experimental details for structural analyses are summarized in Table S1, Supporting Information. Crystallographic material can also be obtained from the CCDC, the deposition numbers being CCDC 862508–862511.

RESULTS AND DISCUSSION

In silver–triazole complexes, bi-³³ and tetranuclear clusters³⁴ are the most widespread structural motifs. For the studied compounds (1–4) the first type $\{\text{Ag}_2(\text{tr})_4\}^{2+}$ is clearly represented in the complex $[\text{Ag}_2(\text{tr}_{2ad})_2](\text{ClO}_4)_2$ (1). Every silver ion of the centrosymmetric binuclear cluster adopts a triangular AgN_3 environment completed by two μ_2 and one monocoordinating triazole ring. Within the pseudo-planar $\{\text{Ag}_2(\text{tr})_4\}^{2+}$ fragment the metal centers are separated by means of the N^1, N^2 -bridge at a distance of 4.0375(9) Å. The organic ligands (*tr*_{2ad}) link neighboring clusters into a 2D rhombohedral grid network (dimensions of the grid are 13.71 × 13.71 Å, and diagonal-to-diagonal distances between the disilver nodes are 18.88 × 19.88 Å, Figure 1). In this case only

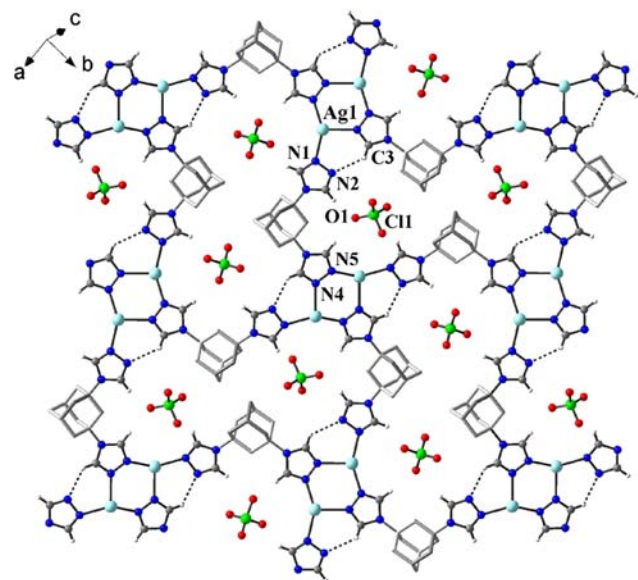


Figure 1. Square net of compound 1: dinuclear silver units act as nodes of the framework, where uncoordinated perchlorate anions occupy the cavities.

three N-donor atoms are used in coordination, while the last one remains uncoordinating, forming the hydrogen bond with the C–H (triazole) group (distance $\text{N}2\text{--C}3$ is 3.17 Å). Such networks are tightly packed, leading to hydrophilic channels with a van der Waals cross section of 2 × 3 Å running along the *a* axis (see Figure S1, Supporting Information). The closest distance between Ag^1 ions of the nearest layers is 3.2827(9) Å, which can be interpreted as a sufficiently strong argentophilic interaction, by a comparison with known Ag–triazole complexes.³⁵ The channel space is occupied with non-coordinating ClO_4^- anions that are involved in hydrogen-bonding and anion $\cdots\pi(\text{tr})$ interactions. In the IR spectrum of compound 1 two bands at 1094 and 624 cm^{-1} can be assigned to stretches of the ClO_4^- anions.

While investigating the $\text{Ag}^1/\text{V}_2\text{O}_5/\text{HF}/\text{tr}$ -ligand systems under hydrothermal conditions we found formation of novel 1,2,4-triazole-supported mixed-metal $\{\text{Ag}_2(\text{VO}_2\text{F}_2)_2(\text{tr})_4\}$

SBUs. In the IR spectra of the obtained compounds it is possible to ascribe the bands at 910–920 cm^{-1} to the symmetric and asymmetric $\text{V}=\text{O}$ stretches, while the stretches of terminal $\text{V}\text{--F}$ bonds are observed at ca. 590 cm^{-1} (according to ref 8a). In the crystal structure of $[\text{Ag}_2(\text{VO}_2\text{F}_2)_2(\text{tr}_{2ad})_2]\cdot\text{H}_2\text{O}$ (2) the silver atoms adopt the distorted tetrahedral environment AgN_3O and are associated with the vanadium oxo–fluoride anions $\{\text{VO}_2\text{F}_2\}^-$ through the triazole and oxo bridges (Figure 2). The bis-triazole ligands are

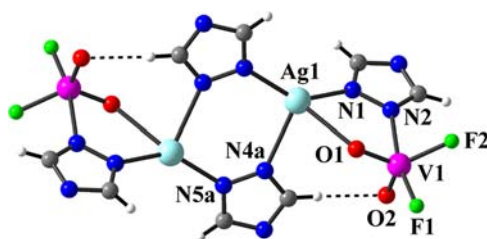


Figure 2. Tetranuclear mixed-metal SBU in complex 2. 1,2,4-Triazole, as a short N,N-bridge, connects two metal ions, forming disilver fragments with further vanadium coordination.

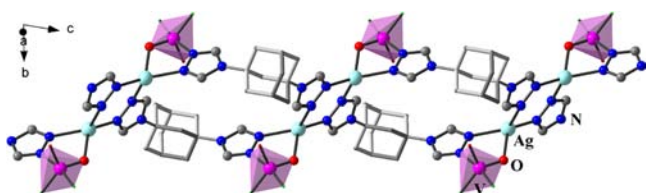
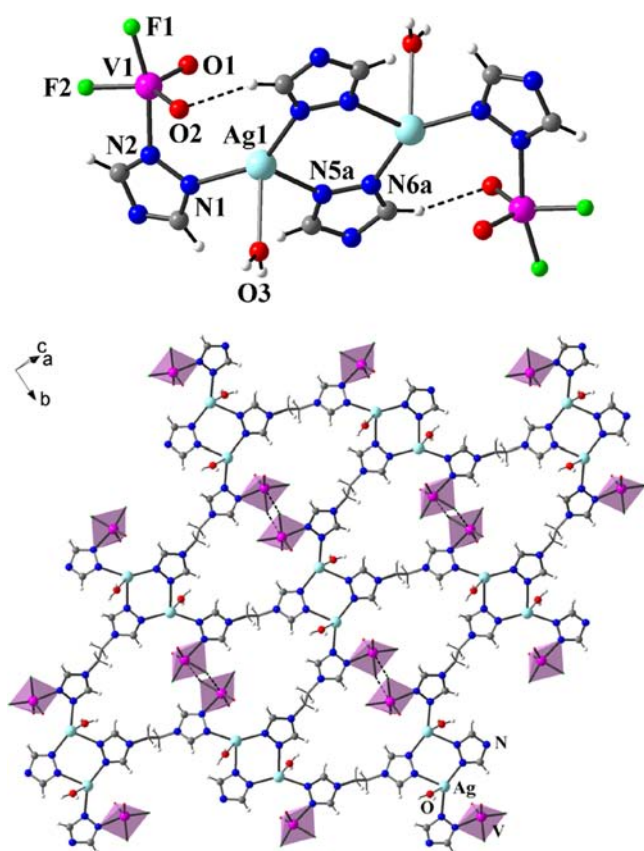
μ_4 coordinating: one functional group links two adjacent silver ions ($\text{Ag}\cdots\text{Ag}$ 4.3633(7) Å), while another one combines silver and vanadium ions at a distance of 3.7997(6) Å. Thereby the vanadium centers possess a five-coordinated environment as a distorted trigonal bipyramid $\text{VO}_2\text{F}_2\text{N}$ (principal geometric parameters are given in Table 2). Such polyhedra can be more precisely described by Reedijk's factor τ of ca. 0.74 ($\tau = 0$ for square pyramid and $\tau = 1$ for trigonal bipyramid³⁶). The angular geometry of the bitopic ligand *tr*_{2ad} facilitates catenation of the SBUs at 12.6 Å (distance between the centers of binuclear silver fragments) by double organic bridges into a 1D coordination polymer (Figure 3). The anionic parts of heterobimetallic clusters are involved in hydrogen bonding with triazoles and solvate water molecules leading to close packing in the crystal.

The structural motif in compound $[\text{Ag}_2(\text{VO}_2\text{F}_2)_2(\text{tr}_{2eth})_2\cdot(\text{H}_2\text{O})_2]$ (3) is slightly different. The tetrahedral environment of the silver atoms AgN_3O is supplemented with a weakly bonded water molecule ($\text{Ag}\text{--O}$ 2.595(3) Å) while being connected with the anionic fragment $\{\text{VO}_2\text{F}_2\}^-$ only through a triazole bridge. The IR spectrum of 3 is clearly representative, showing two strong bands at 910 and 878 cm^{-1} from terminal $\text{V}=\text{O}$ stretches. Assuming a linear geometry in the crystal lattice, the bitopic organic ligand (*tr*_{2eth}), as a μ_4 -linker, organizes the heterobimetallic SBUs into a square net (the shortest distance between the centers of tetranuclear units within the sheet is 13.2 Å) (Figure 4). Between the layers, the inorganic clusters are located close to one another at a distance of 4.05 Å, which causes the distant double $\text{V}^{\delta+}\text{--F}^{\delta-}$ interaction of 2.842(4) Å between two anionic parts (Figure S5, Supporting Information). The coordination environment of the vanadium atoms can be described as a distorted tetragonal bipyramid ($\tau = 0.44$) with one elongated bond. The hydrogen bonding between the coordinated water molecule and the vanadium oxo–fluoride unit ($\text{O}_w\text{--O}_{\text{anion}}$ is 2.76 Å) promotes tight parallel packing of planar nets.

The same principle is realized with 1,4-bis(1,2,4-triazol-4-yl)cyclohexane in coordination polymer $[\text{Ag}_2(\text{VO}_2\text{F}_2)_2(\text{tr}_{2cy})_2]\cdot 4\text{H}_2\text{O}$ (4). Similarly to complex 2, the coordination environment AgN_3O is completed with vanadium

Table 2. Principal Geometric Parameters (Angstroms, degrees) of Heterobimetallic Fragments in Compounds 2–4

	[Ag ₂ (VO ₂ F ₂) ₂ (tr ₂ ad) ₂].H ₂ O (2)	[Ag ₂ (VO ₂ F ₂) ₂ (tr ₂ eth) ₂ (H ₂ O) ₂] (3)	[Ag ₂ (VO ₂ F ₂) ₂ (tr ₂ cy) ₂].4H ₂ O (4)
V=O	1.6390(15), 1.669(2)	1.639(3), 1.650(4)	1.616(3), 1.639(2)
V–F	1.8365(15), 1.8400(15)	1.866(3), 1.890(3)	1.841(2), 1.8837(19)
V–N _{tr}	2.1826(17)	2.147(3)	2.133(2)
Ag–N _{tr}	2.2088(16)–2.464(2)	2.212(3)–2.445(3)	2.178(2)–2.520(3)
Ag–O	2.5578(16)	2.595(3)	2.667(3)
Ag...V	3.7997(6)	3.8132(8)	3.7400(6)
Ag...Ag (dimer)	4.3633(7)	4.2745(6)	4.2384(5)
O=V=O	110.59(9)	107.54(17)	109.95(15)
O=V–F	99.37(8), 100.08(10) ^{ax}	97.8(2), 99.33(16) ^{ax}	96.85(11), 99.69(11) ^{ax}
F–V–F	120.93(8), 125.69(9) ^{eq}	111.00(17), 139.69(16) ^{eq}	121.80(13), 126.81(14) ^{eq}
F–V–F	88.07(7)	86.87(12)	86.31(10)
O=V–N	86.65(7), 87.45(8)	88.60(13), 90.33(15)	89.44(11), 89.80(12)
F–V–N	79.91(7), 167.90(8)	79.90(11), 166.28(14)	79.78(10), 166.06(10)
N–Ag–N	100.23(6)–142.35(6)	103.45(10)–145.03(11)	92.12(9)–161.37(9)

Figure 3. Catenation of Ag/VOF SBUs into 1D coordination polymer 2 by means of double organic bridge tr₂ad.Figure 4. Heterobimetallic Ag/VOF unit with additionally coordinated water molecule in complex 3 that is connected with linear triazole ligands tr₂eth into a 2D square net.

oxo–fluoride anions as a distant bonding contact Ag–O_{anion} 2.667(3) Å. The IR spectrum shows one strong band at 916

cm⁻¹ from V=O stretching vibration. The value of Reedijk's factor (ca. 0.65) reveals a distorted trigonal bipyramidal geometry for the five-coordinated vanadium ions (O₂F₂N). The trans-1,4-disubstituted cyclohexane derivative adopts the most profitable chair configuration that supports the equatorial–equatorial (e,e) disposition of the triazole heterocycles rather than an alternative axial–axial (a,a) conformation.³⁷ At the same time, the tr rings are orthogonally arranged to the aliphatic core. As a linear connector, tr₂cy bridges heterobimetallic fragments into 2D square nets at a distance of 14.43 Å (Figure 5), which are closely packed at the expense of hydrogen bonding.

In hydrothermal reactions the V^{+V} forms can be easily reduced to V^{+IV} and even V^{+III}.⁵ According to valence bond calculations, in 2–4 the oxidation state +V is realized (Table 3). Comparing the crystal structure data with the results of such

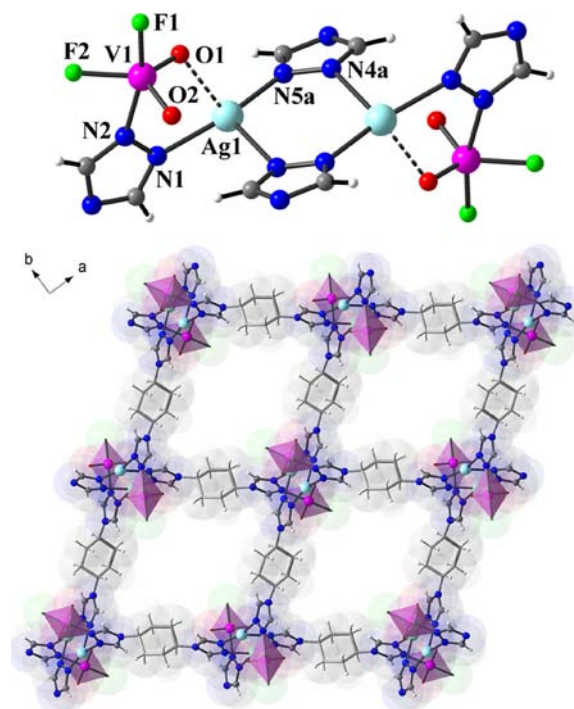


Figure 5. Ag/VOF building fragment as a node of the 'square grid' framework topology with linear triazolyl linkers in the crystal structure of 4.

Table 3. Bond Valence Sums for $\{\text{VO}_2\text{F}_2\text{N}\}^-$ Units in the Heterobimetallic Complexes^a

	$[\text{Ag}_2(\text{VO}_2\text{F}_2)_2(\text{tr}_2\text{ad})_2]\cdot\text{H}_2\text{O}$ (2)			$[\text{Ag}_2(\text{VO}_2\text{F}_2)_2(\text{tr}_2\text{eth})_2(\text{H}_2\text{O})_2]$ (3)			$[\text{Ag}_2(\text{VO}_2\text{F}_2)_2(\text{tr}_2\text{cy})_2]\cdot 4\text{H}_2\text{O}$ (4)		
	R_i , Å	S_i	$V - S_i$	R_i , Å	S_i	$V - S_i$	R_i , Å	S_i	$V - S_i$
V–O1	1.6390(15)	1.55	0.45 ^b	1.650(4)	1.51	0.49 ^c	1.616(3)	1.66	0.34 ^b
V–O2	1.669(2)	1.43	0.57 ^c	1.639(3)	1.56	0.44 ^c	1.639(2)	1.55	0.45 ^c
V–F1	1.8400(15)	0.71	0.29	1.866(3)	0.66	0.34	1.8837(19)	0.63	0.37 ^c
V–F2	1.8365(15)	0.71	0.29	1.890(3)	0.62	0.38 ^d	1.841(2)	0.70	0.30 ^c
V–N _{tr}	2.1826(17)	0.45		2.147(3)	0.50		2.133(2)	0.52	
		$\sum S_i = 4.85$			$\sum S_i = 4.85$			$\sum S_i = 5.06$	

^aValence sums were calculated with the formula $S_i = \exp[(R_0 - R_i)/B]$ (S_i , bond valence of bond “ i ”; R_0 , constant dependent on the bonded element; R_i , length of bond “ i ”; $B = 0.370$). $\sum S_i$, bond valence sum for vanadium. V , predicted valence for a site. R_0 (V–O) = 1.803 Å, R_0 (V–F) = 1.710 Å, R_0 (V–N) = 1.889 Å. ^bBond to Ag^+ . ^cH-bond acceptor. ^dElongated contact V–F.

calculations there are some correlations between the bond lengths in vanadium oxo–fluoride anions and their hydrogen bonding in the crystal. Atoms with the highest partial negative charges ($V - S_i$) have a tendency either for coordination to metal centers or for H-bond accepting, as is clearly observed in compound 2. Thus, two oxygen atoms O1 and O2 have partial negative charges of 0.45 and 0.57, respectively, which is a result of their higher nucleophilic ability, leading to distal bonds to silver ions and hydrogen bonds with C–H groups of triazole heterocycles (O–C = 3.08–3.12 Å). In compounds 3 and 4 the hydrogen-bond network is more complicated, including solvate water molecules and triazole moieties; therefore, almost all O and F atoms of VOF anions are involved in H-bonding patterns as reflected in the partial negative charge calculations (Table 3).

Thermal Stability. The thermal behavior of complexes 1, 2, and 4 was studied using temperature-dependent powder X-ray diffractometry (TD PXRD) in a capillary under argon atmosphere (Figures S15 and S16, Supporting Information). According to the diffraction patterns, compounds 1 and 2 remain stable up to 300 °C. In the case of compound 4 the thermal behavior is more complicated. The structure is invariable until 160 °C; then the reflection angles are shifted caused by removal of the solvate water molecules located between the metal–organic layers. The Guinier–Simon diagram reveals three phase transitions in the temperature range up to 280 °C. Total decomposition of substances occurs at 300 °C accompanied by crystallization of silver in the face-centered cubic lattice.

Photoluminescence Properties. The synthesized compounds show an extended absorption in the UV–vis range. The room-temperature diffuse reflectance spectra of free ligands are shown in Figure 6, curves a–c. Spectra are very similar with two maxima at ca. 320 and ca. 250 nm and a strong UV absorption band starting at ca. 220 nm. Curves d–g in Figure 6 present the reflectance spectra recorded for compounds 1–4. Spectra of 2–4 are dominated by the strong absorption band of VO_2F_2^- , responsible for the yellowish color of these AgVOFs. The compound $[\text{Ag}_2(\text{tr}_2\text{ad})](\text{ClO}_4)_2$ (1) has no absorption band in a visible range. The most striking feature of its spectrum is the absence of the absorption band observed for the free tr_2ad ligand at 320 nm. Moreover, the absorption bands of 1 seem to be slightly red shifted as compared to those of free ligand.

The solid state luminescence spectra of free ligands and complexes 1–4 were examined at 298 and 77 K. The tr_2ad ligand and compound 1 are luminescent at room temperature, while for tr_2cy a weak luminescence could be noticed only at 77 K. In contrast, the tr_2eth ligand as well as compounds 2–4 are not luminescent even after cooling them to liquid nitrogen temperature. The possible tr_2eth fluorescence is apparently

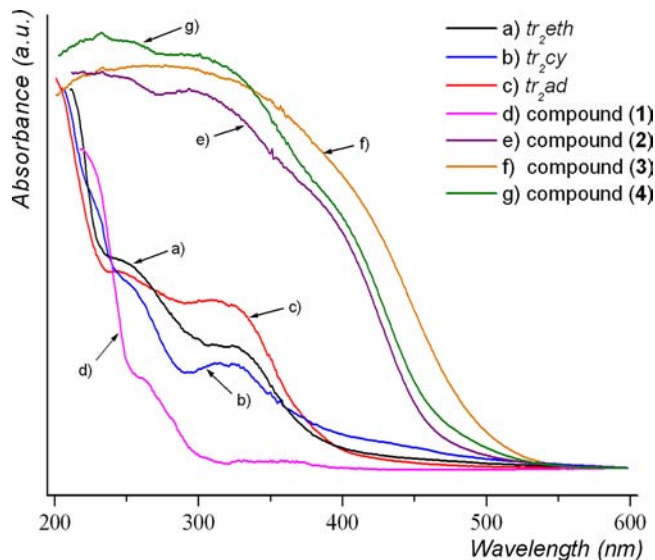


Figure 6. Diffuse reflectance spectra of free ligands and complexes 1–4.

quenched by the thermal rotations of triazole rings around the C–C and C–N bonds. The intraligand fluorescence was observed for tr_2eth after its immobilization in a coordination network,³⁸ which stops rotation and freezes a single conformation. It seems that a similar effect is responsible for observed tr_2ad emission. The 1,2,4-triazole rings are connected by rigid angular 1,3-adamantandiyli, which increases the ligand conformational stiffness, thereby reducing the nonradiative decay of the intraligand ($\pi-\pi^*$) excited state. This is not the case for the tr_2eth ligand with a flexible 1,2-ethanediyli linker.

Figure 7 presents the emission and excitation spectra recorded for tr_2ad and compound 1. Emission of 1 at 77 K is more intense than at 298 K, and the bands are a little better resolved. Both the emission and the excitation bands are very similar for the free tr_2ad ligand and compound 1, and only the small shift of the band positions toward longer wavelengths can be noticed for the latter. The maximum of the excitation band is observed at 285 nm for tr_2ad and 290 nm for 1. Emission spectra show vibronic structure with maxima at 412, 438, and 460 nm for tr_2ad and at 418, 442, 463, and 486 nm for 1. The observed vibrational progression spacings of ca. 1100–1440 cm^{-1} for tr_2ad and ca. 1020–1300 cm^{-1} for 1 suggest that the emission of complex 1 arises from a ligand-centered transitions. The inset in Figure 7 shows the emission decay curves recorded at 77 K for tr_2ad ligand and compound 1. In both cases the decay curves are biexponential with the major contribution

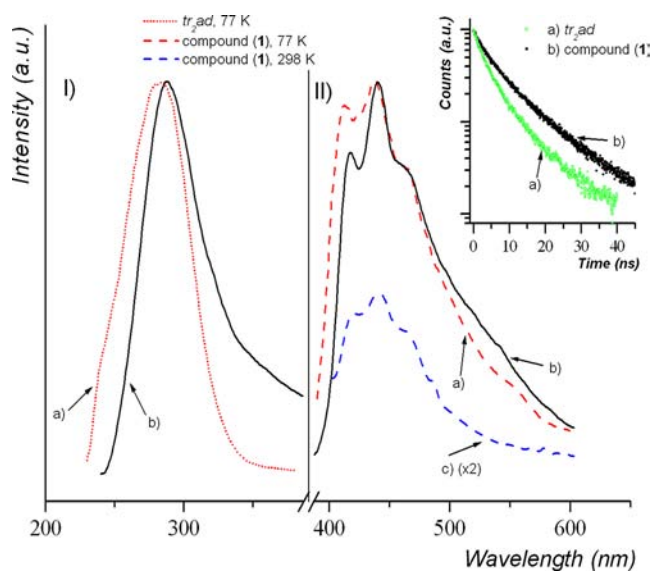


Figure 7. Excitation (I) ($\lambda_{\text{em}} = 440$ nm) and emission (II) ($\lambda_{\text{ex}} = 290$ nm) spectra recorded for tr_2ad at 77 K (a), compound **1** at 77 K (b), and compound **1** at 298 K (c). (Inset) Emission decay curves recorded for tr_2ad (a) and **1** (b) at 77 K.

from the longer component. The determined time constants are $t_1 = 2.5$ ns, $t_2 = 8.3$ ns for tr_2ad and $t_1 = 4.8$ ns, $t_2 = 14.6$ ns for **1**. The almost two times increase in the decay times observed for **1** may result from the less efficient nonradiative relaxation process due to the larger rigidity of the ligand surrounding in the coordination frameworks.

The emission bands of tr_2ad should be assigned as $n-\pi^*$ or $\pi-\pi^*$ transitions. On the basis of MO calculations (see Supporting Information, density functional theory (DFT) computations) and the observed similarity of the excitation and emission bands of the free ligand and the complex, the emission of compound **1** may be assigned to originate from intraligand $\pi-\pi^*$ transitions.

For d^{10} metal complexes besides the ligand-centered $\pi-\pi^*$ transitions the ligand-to-metal or metal-to-ligand (LMCT or MLCT) charge-transfer transitions are possible.³⁹ Furthermore, the Ag^+ ion can exert a heavy-atom effect on the ligand, leading to the intraligand phosphorescence.⁴⁰ The emission originating from the $^3[\pi-\pi^*]$ excited state of the $Ag(I)$ complex with 3,5-disubstituted-1,2,4-triazole was reported in the literature.³⁵ However, the decay time of $^3[\pi-\pi^*]$ phosphorescence should be considerably longer than that observed for complex **1**. Moreover, cooling of complex **1** to 77 K led to enhancement of the emission intensity but without any change in the band profile. Our MO calculations on **1** show that orbitals with energies close to the HOMO and LUMO do not have contributions from the Ag^+ ion. Therefore, in our case the LMCT or MLCT can be excluded for complex **1**.

Complexes **2–4** do not show any luminescence. The broad absorption bands (Figure 6), which should be assigned as LMCT (L–V(d)) transitions of vanadium oxo–fluoride, are observed for these complexes at energy lower than the energy of $n-\pi^*$ ($\pi-\pi^*$) transitions of ligands. Luminescence is observed for $[Ag_2(tr_2ad)](ClO_4)_2$ (**1**) but is not present for $[Ag_2(VO_2F_2)_2(tr_2ad)_2] \cdot H_2O$ (**2**) containing the same tr_2ad ligand. Hence, most probably the emission quenching of **2–4** results from the presence of the $\{VO_2F_2\}^-$ anion in the crystal structure of these complexes, which provides an additional path

for nonradiative relaxation (e.g., through intersystem crossing, ISC). A similar effect of oxovanadium VO_2^+ cation on emission quenching of pyridyl/pyrimidyl–pyrazole-derived ditopic ligands has been reported recently.⁴¹

CONCLUSION

In the present study we demonstrated a rational design approach for construction of heterobimetallic AgVOF frameworks utilizing the unique coordination potential of bifunctional 1,2,4-triazoles. Unprecedentedly, in the discrete $[Ag_2(VO_2F_2)_2(tr)_4]$ cluster architecture four triazole heterocycles elegantly connect two diverse metal centers in pairs ($Ag \cdots V$ 3.74–3.81 Å), affording the zigzag V–Ag–Ag–V sequence. The design principle opens an efficient pathway to the mixed-metal AgVOF materials with high thermal stability and interesting photochemical properties. Apparently, the approach can also be applied to other heterocyclic systems (1,2,3-triazoles, tetrazoles, etc.). Photoluminescence of the tr_2ad ligand originates from $n-\pi^*$ or $\pi-\pi^*$ transitions, while luminescence of $[Ag_2(tr_2ad)](ClO_4)_2$ is due to ligand-centered $\pi-\pi^*$ transitions. Such intraligand emission is quenched, however, if the $\{VO_2F_2\}^-$ anion is incorporated into the complex structure.

ASSOCIATED CONTENT

Supporting Information

X-ray crystallographic data of **1–4** in CIF format, crystallographic data and experimental details for X-ray structural analyses, spectral characterization data, XRPD, thermo-XRPD diffractograms, and DFT computations. This material is available free of charge via the Internet at <http://pubs.acs.org>.

AUTHOR INFORMATION

Corresponding Author

*E-mail address: ab_lysenko@univ.kiev.ua.

Notes

The authors declare no competing financial interest.

ACKNOWLEDGMENTS

Financial support by Deutsche Forschungsgemeinschaft is gratefully acknowledged.

REFERENCES

- (1) Tranchemontagne, D. J.; Mendoza-Cortes, J. L.; O’Keeffe, M.; Yaghi, O. M. *Chem. Soc. Rev.* **2009**, *38*, 1257.
- (2) (a) Dolbecq, A.; Dumas, E.; Mayer, C. R.; Mialane, P. *Chem. Rev.* **2010**, *110*, 6009. (b) Shubert, U. *Chem. Soc. Rev.* **2011**, *40*, 575. (c) Allendorf, M. D.; Bauer, C. A.; Bhakta, R. K.; Houk, R. J. T. *Chem. Soc. Rev.* **2009**, *38*, 1330. (d) Cui, Y.; Yue, Y.; Qian, G.; Chen, B. *Chem. Rev.* **2012**, *112*, 1126.
- (3) Adil, K.; Leblanc, M.; Maisonneuve, V.; Lightfoot, P. *Dalton Trans.* **2010**, *39*, 5983.
- (4) Reiskamp, H.; Mattes, R. *Z. Naturforsch.* **1976**, *B31*, 1453.
- (5) Aldous, D. W.; Stephens, N. F.; Lightfoot, P. *Dalton Trans.* **2007**, 2271.
- (6) Stephens, N. F.; Buch, M.; Lightfoot, P. *J. Mater. Chem.* **2005**, *15*, 4298.
- (7) Aldous, D. W.; Stephens, N. F.; Lightfoot, P. *Dalton Trans.* **2007**, 4207.
- (8) (a) Bukovec, P.; Milicev, S.; Demsar, A.; Golic, L. *J. Chem. Soc., Dalton Trans.* **1981**, 1802. (b) Darriet, J.; Xu, Q.; Tressaud, A. *Acta Crystallogr.* **1987**, *C43*, 224.
- (9) Demsar, A.; Bukovec, P. *Croat. Chem. Acta* **1984**, *57*, 673.

- (10) Buchholz, N.; Leimkühler, M.; Mattes, R. *Eur. Cryst. Meeting* **1985**, *9*, 134.
- (11) Buchholz, N.; Leimkühler, M.; Kiriazis, L.; Mattes, R. *Inorg. Chem.* **1988**, *27*, 2035.
- (12) Hilbers, M.; Leimkühler, M.; Mattes, R. *Z. Naturforsch.* **1989**, *B44*, 383.
- (13) Ninclaus, C.; Riou, D; Ferey, G. *Chem. Commun.* **1997**, 851.
- (14) Aidoudi, F. H.; Byrne, P. J.; Allan, P. K.; Teat, S. J.; Lightfoot, P.; Morris, R. E. *Dalton Trans.* **2011**, *40*, 4324.
- (15) Aldous, D. W.; Slawin, A. M. Z.; Lightfoot, P. *Acta Crystallogr.* **2010**, *C66*, m130.
- (16) Himeur, F.; Allan, P. K.; Teat, S. J.; Goff, R. J.; Morris, R. E.; Lightfoot, P. *Dalton Trans.* **2010**, *39*, 6018.
- (17) Aldous, D. W.; Goff, R. J.; Attfield, J. P.; Lightfoot, P. *Inorg. Chem.* **2007**, *46*, 1277.
- (18) Welk, M. E.; Norquist, A. J.; Stern, C. L.; Poeppelmeier, K. R. *Inorg. Chem.* **2000**, *39*, 3946.
- (19) Welk, M. E.; Stern, C. L.; Poeppelmeier, K. R.; Norquist, A. J. *Cryst. Growth Des.* **2007**, *7*, 956.
- (20) Mahenthirarajah, T.; Lightfoot, P. *Chem. Commun.* **2008**, 1401.
- (21) Mahenthirarajah, T.; Li, Y.; Lightfoot, P. *Inorg. Chem.* **2008**, *47*, 9097.
- (22) Davis, M. F.; Jura, M.; Leung, A.; Levason, W.; Littlefield, B.; Reid, G.; Webster, M. *Dalton Trans.* **2008**, 6265.
- (23) Davis, M. F.; Levason, W.; Paterson, J.; Reid, G.; Webster, M. *Eur. J. Inorg. Chem.* **2008**, 802.
- (24) Edwards, A. J.; Slim, D. R.; Guerchais, J. E.; Sala-Pala, J. J. *Chem. Soc., Dalton Trans.* **1977**, 984.
- (25) DeBurgomaster, P.; Zubieta, J. *Acta Crystallogr.* **2010**, *E66*, m1303.
- (26) (a) Sorensen, E. M.; Izumi, H. K.; Vaughey, J. T.; Stern, C. L.; Poeppelmeier, K. R. *J. Am. Chem. Soc.* **2005**, *127*, 6347. (b) Albrecht, T. A.; Sauvage, F.; Bodenez, V.; Tarascon, J.-M.; Poeppelmeier, K. R. *Chem. Mater.* **2009**, *21*, 3017.
- (27) Chamberlain, J. M.; Albrecht, T. A.; Lesage, J.; Sauvage, F.; Stern, C. L.; Poeppelmeier, K. R. *Cryst. Growth Des.* **2010**, *10*, 4868.
- (28) Lin, H.; Maggard, P. A. *Inorg. Chem.* **2008**, *47*, 8044.
- (29) (a) Dong, P.; Zhang, Q.-K.; Wang, F.; Chen, S.-C.; Wu, X.-Y.; Zhao, Z.-G.; Lu, C.-Z. *Cryst. Growth Des.* **2010**, *10*, 3218. (b) Tripuramallu, B. K.; Kishore, R.; Das, S. K. *Inorg. Chim. Acta* **2011**, *368*, 132. (c) Yang, M.-X.; Lin, S.; Chen, L.-J.; Zhang, X.-F.; Huang, H. *Inorg. Chem. Commun.* **2011**, *14*, 1652.
- (30) (a) Lysenko, A. B.; Senchyk, G. A.; Lincke, J.; Lässig, D.; Fokin, A. A.; Butova, E. D.; Schreiner, P. R.; Krautscheid, H.; Domasevitch, K. V. *Dalton Trans.* **2010**, *39*, 4223. (b) Senchyk, G. A.; Lysenko, A. B.; Krautscheid, H.; Domasevitch, K. V. *Inorg. Chem. Commun.* **2011**, *14*, 1365.
- (31) Senchyk, G. A.; Lysenko, A. B.; Rusanov, E. B.; Chernega, A. N.; Krautscheid, H.; Domasevitch, K. V. *Inorg. Chim. Acta* **2009**, *362*, 4439.
- (32) Sheldrick, G. M. *Acta Crystallogr.* **2008**, *A64*, 112.
- (33) Wang, Y.; Ding, B.; Cheng, P.; Liao, D.-Z.; Yan, S.-P. *Inorg. Chem.* **2007**, *46*, 2002.
- (34) (a) Wang, Y.; Yi, L.; Yang, X.; Ding, B.; Cheng, P.; Liao, D.-Z.; Yan, S.-P. *Inorg. Chem.* **2006**, *45*, 5822. (b) Liu, B.; Xu, L.; Guo, G.-C.; Huang, J.-S. *Inorg. Chem. Commun.* **2006**, *9*, 687.
- (35) Zhang, J.-P.; Lin, Y.-Y.; Huang, X.-C.; Chen, X.-M. *J. Am. Chem. Soc.* **2005**, *127*, 5495.
- (36) Addison, A. W.; Rao, T. N.; Reedijk, J.; Rijn, J. V.; Verschoor, G. C. *J. Chem. Soc., Dalton Trans.* **1984**, 1349.
- (37) Zheng, Y.-Z.; Speldrich, M.; Kögerler, P.; Chen, X.-M. *CrystEngComm* **2010**, *12*, 1057.
- (38) Habib, H. A.; Hoffmann, A.; Höpfe, H. A.; Steinfeld, G.; Janiak, C. *Inorg. Chem.* **2009**, *48*, 2166.
- (39) Vogler, A.; Kunkely, H. *Top. Curr. Chem.* **2001**, *213*, 143.
- (40) Kunkely, H.; Vogler, A. *Inorg. Chem. Commun.* **2006**, *9*, 866.
- (41) Mandal, T. N.; Roy, S.; Gupta, S.; Paul, B. K.; Butcher, R. J.; Rheingold, A. L.; Kar, S. K. *Polyhedron* **2011**, *30*, 1595.